CHAPTER II
SYNTHESIS AND CHARACTERIZATION

CHAPTER - II
SYNTHESIS AND CHARACTERIZATION

PART - A : SYNTHESIS OF FERRITES

INTRODUCTION

Ferrites are structure sensitive materials. 1,2,3 Their properties severely depend on differences in the manufacturing process.

The investigations on solid state reaction leading to the formation of ferrite began as early as 1909 by Hilpert.[4] Hedvall[5], Tammann[6] and Jandar[7] contributed much to the understanding of ferrite reaction. The modern theory of preparation of spinel ferrite has been introduced by Wanger.[8]

The numbers of methods have been developed for the preparation of ferrites. Most of the parameters required for any particular application often depend on the method of preparation. The properties of ferrites are the consequence of their internal structure and are highly influenced by heat treatment, crystal structure and cation distribution. The grain size, porosity, density, orientation of grains etc. also play a very important role in deciding their properties.

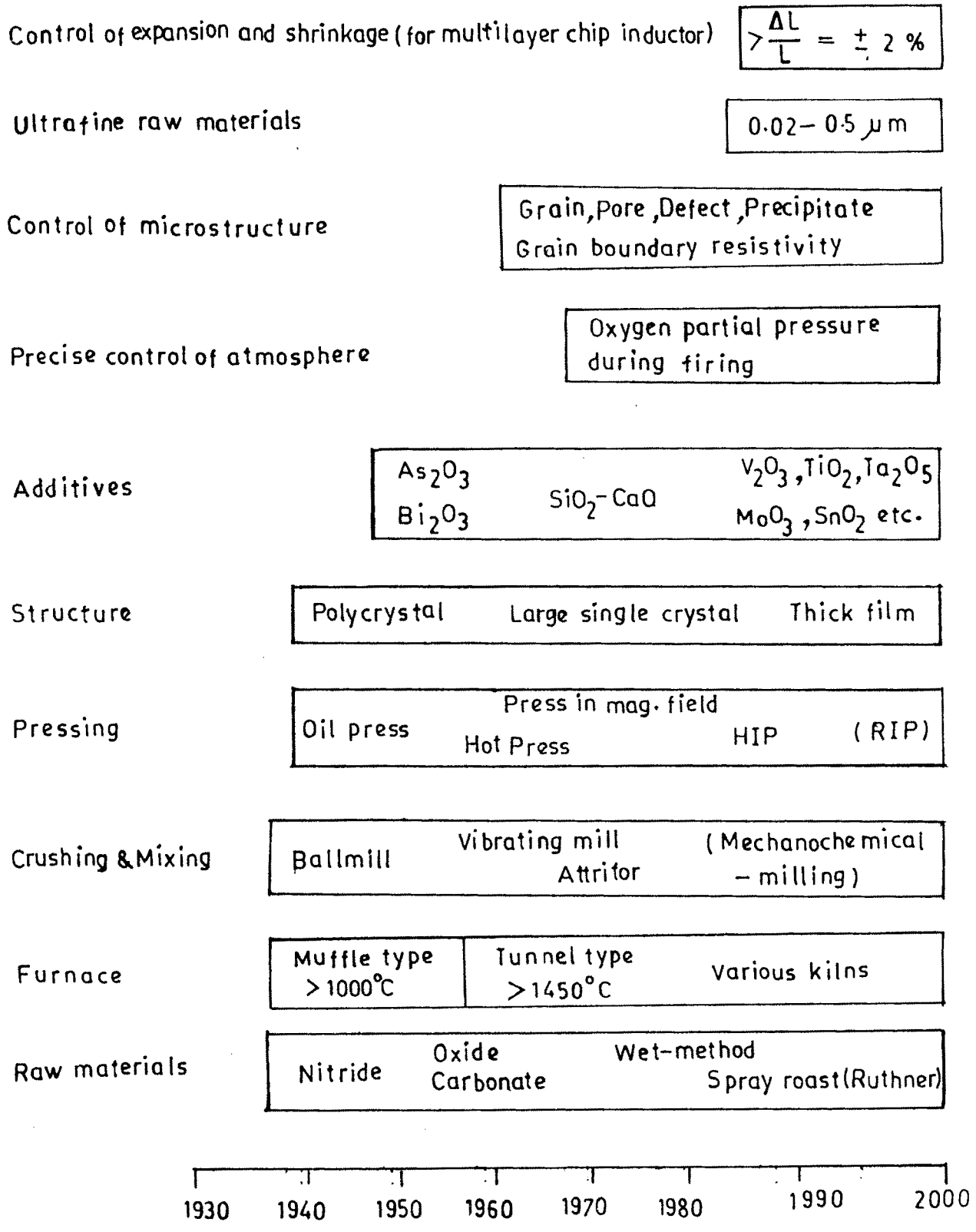Basically there are four steps in the preparation of ferrites.

Control of expansion and shrinkage (for multilayer chip inductor)

$$\dfrac{\Delta L}{L} = \pm 2\%$$

Ultrafine raw materials

0.02 – 0.5 μm

Control of microstructure

Grain, Pore, Defect, Precipitate
Grain boundary resistivity

Precise control of atmosphere

Oxygen partial pressure
during firing

Additives

As_2O_3 Bi_2O_3 SiO_2–CaO V_2O_3, TiO_2, Ta_2O_5 MoO_3, SnO_2 etc.

Structure

Polycrystal   Large single crystal   Thick film

Pressing

Press in mag. field
Oil press   Hot Press   HIP   (RIP)

Crushing & Mixing

Ballmill   Vibrating mill   Attritor   (Mechanochemical – milling)

Furnace

Muffle type >1000°C | Tunnel type >1450°C | Various kilns

Raw materials

Nitride | Oxide Carbonate | Wet-method Spray roast (Ruthner)

1930   1940   1950   1960   1970   1980   1990   2000

Fig. 2·A·1 — AN OUTLINE OF DEVELOPMENT OF MANUFACTURING
TECHNOLOGIES OF FERRITES.

1.   Preparation of material to form an intimate mixture in the desired composition.

2.   Presintering and calcination.

3.   Converting the raw ferrite into powder and pressing the powder into the desired shape.

4.   Sintering to produce a highly densified product.

An outline of development of manufacturing technologies of ferrite is shown in Fig. 2A.1.

2.A.1   METHODS OF PREPARATION OF FERRITES

The general methods for the preparation of ferrite compositions are-

2A.1.1   Ceramic Method

This is most extensively used method in the commercial production of ferrites. High purity divalent metal oxide and ferric oxide are mixed together in the required proportion in wet medium. The mixture is presintered at an elevated temperature to form the ferrite powder. The powder is dried, pressed into a suitable shape and final sintered. The flow chart representing the various stages in the preparation of ferrites is shown in Fig. 2.A.2.

2A.1.2   Decomposition Method

Instead of using oxides as starting materials, the salts like carbonates, nitrates and oxalates are used in this method. The salts
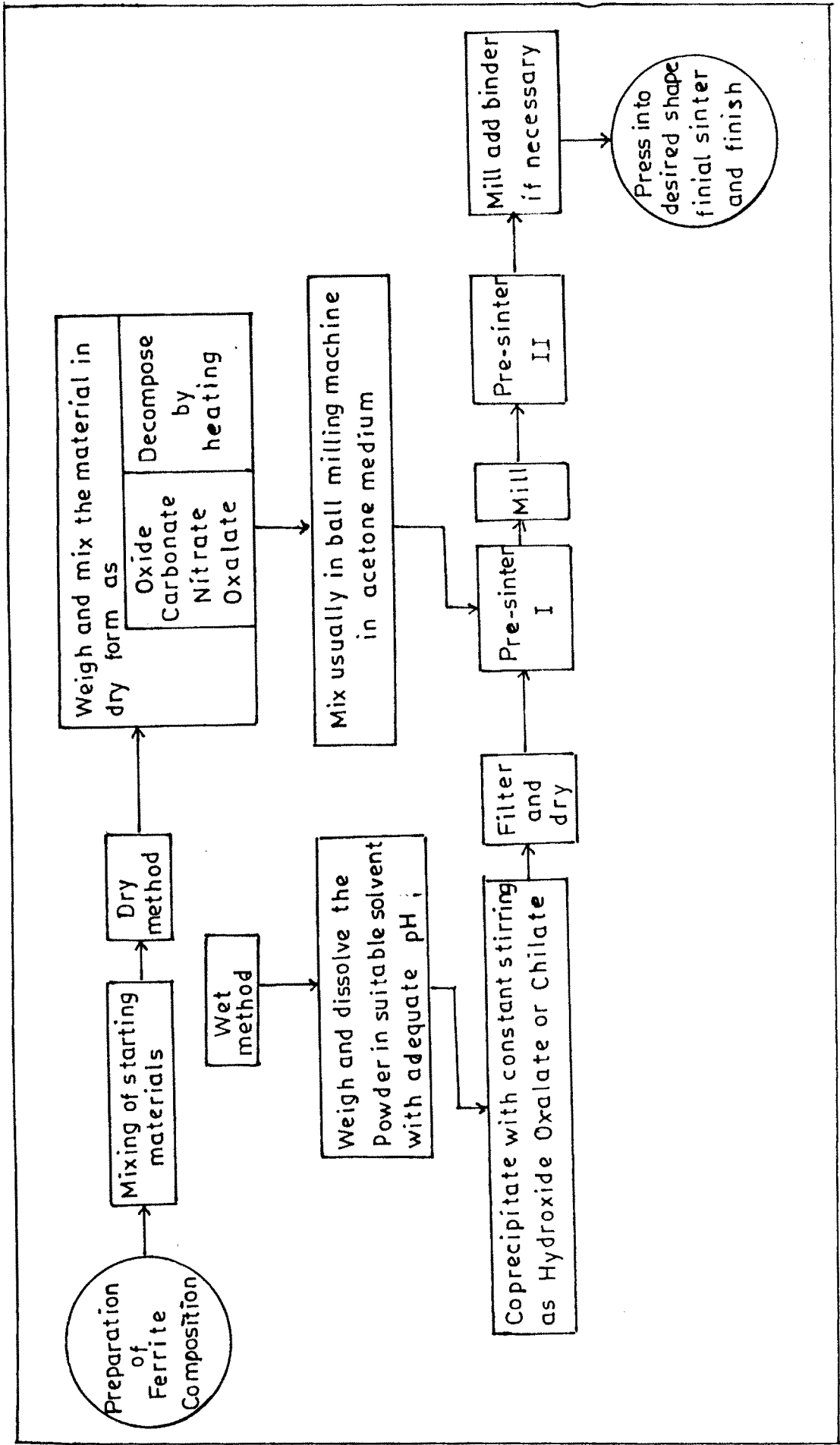
FIG. 2·A·2—FLOW CHART OF STAGES IN THE FERRITE PREPARATION.

are milled in the required proportions and pre-heated in air to produce oxides by thermal decomposition. The preparation undergoes solid state reactions.

2A.1.3 Co-precipitation Method

Co-precipitation method involves the process of mixing the solutions of soluble salts of divalent metal and pure ferric chloride solution in a desired molar proportion. As the cations are mixed on the molecular level, the method is more effective than others. Co-precipitation is an economical way in the production of ultrafine powders.

A. Hydroxide Precipitation Method

To avoid the lengthy milling process involved in dry mixing, attempts have been made to precipitate simultaneously the required hydroxides from a solution.

Economus[12] established this method for the preparation of ferrites. Wolf and Rodrigue[13] used this method for preparation of YIG. Ultrafine spinel ferrites are prepared by Sato and his co-workers who also studied their properties.[14,15]

B. Oxalate Precipitation Method

Precipitation of metallic oxalates is selected for two reasons. The first reason is that precipitation can be carried out using

ammonium oxalates, which does not leave any residue after heating. Secondly most of the metal oxides are very similar in crystal structure. Hence mixing in correct ratio can be achieved on a molecular scale. If the precipitation occurs at widely different rates, mixed crystals do not form uniformly.

C.   Chelate Precipitation Method

Busev[16] and others have prepared ferrites by this method. Chelate are the organo-metallic compounds. Some of these compounds are unstable and insoluble in water. Even then they can be co-precipitated and reduced to ferrite after calcining. This method gives the ferrite powder of constant composition.

2.A.2   SINTERING

This is the most important heat treatment process which severely affects the uniformity of characteristics and dimensions of ferrites. The sintering process has advanced from manual control to automatic control to computer-aided control[17], by which compact is transformed into a dense object. The control of oxygen partial pressure in the sintering process is important. There are two steps of sintering - presintering and final sintering.

2.A.2.1 Presintering

Swallow and Jorden[18] mentioned the purpose of presintering. The purpose of presintering is to -

i.   decompose carbonates and higher oxides thereby reducing the evaluation of gas in the final sintering process.

ii.   assist in homogenization of material.

iii. reduce the effect of variation in the composition of raw materials.

iv.   avoid the shrinkage of the material during the final sintering.

During this process solid state reaction take place and the raw materials partly react to produce the final product. The rate of reaction depends upon the reactivity of the components as well as presintering temperature.

2.A.2.2 Final Sintering

Final sintering helps to develop the microstructure of ferrites. For good quality ferrite the grain size should be uniform. This can be achieved in the final sintering.

The final sintering involves heating the pressed material to a temperature of about 1100-1300 ^{0}C. The formation of brittle solids and the random distribution of ions over A and B sites is avoided by slow cooling rate. The final microstructure together with correct

oxygen content and cation distribution depends upon time and temperature of sintering. During final sintering densification and grain growth occur simultaneously giving rise to variety of micro structures.[19] Extensive reviews on grain growth and sintering are availeble.[20]

2.A.2.3 Sintering Atmosphere

The careful control of sintering atmosphere is very important as it affects the exact proportion of metal ions and also the correct valancy in the final product. It is found that the oxygen deficiency causes iron and some other ions to exist in more than one valance states. Excess of oxygen will result in the formation of cation vacancies.

2.A.3   SOLID STATE REACTION

The mechanism of ferrite formation by solid state reaction has been discussed by several authors[21-23] on the basis of simple diffusion couple involving divalent metal oxide and Fe_2O_3 as shown in Fig. 2.A.3. The ceramic process is governed by the solid state reaction at high temperature viz.

$$MO + Fe_2O_3 \longrightarrow MFe_2O_4 \qquad \qquad ... \qquad (2.1)$$
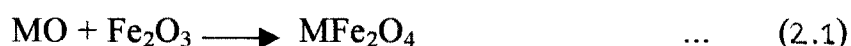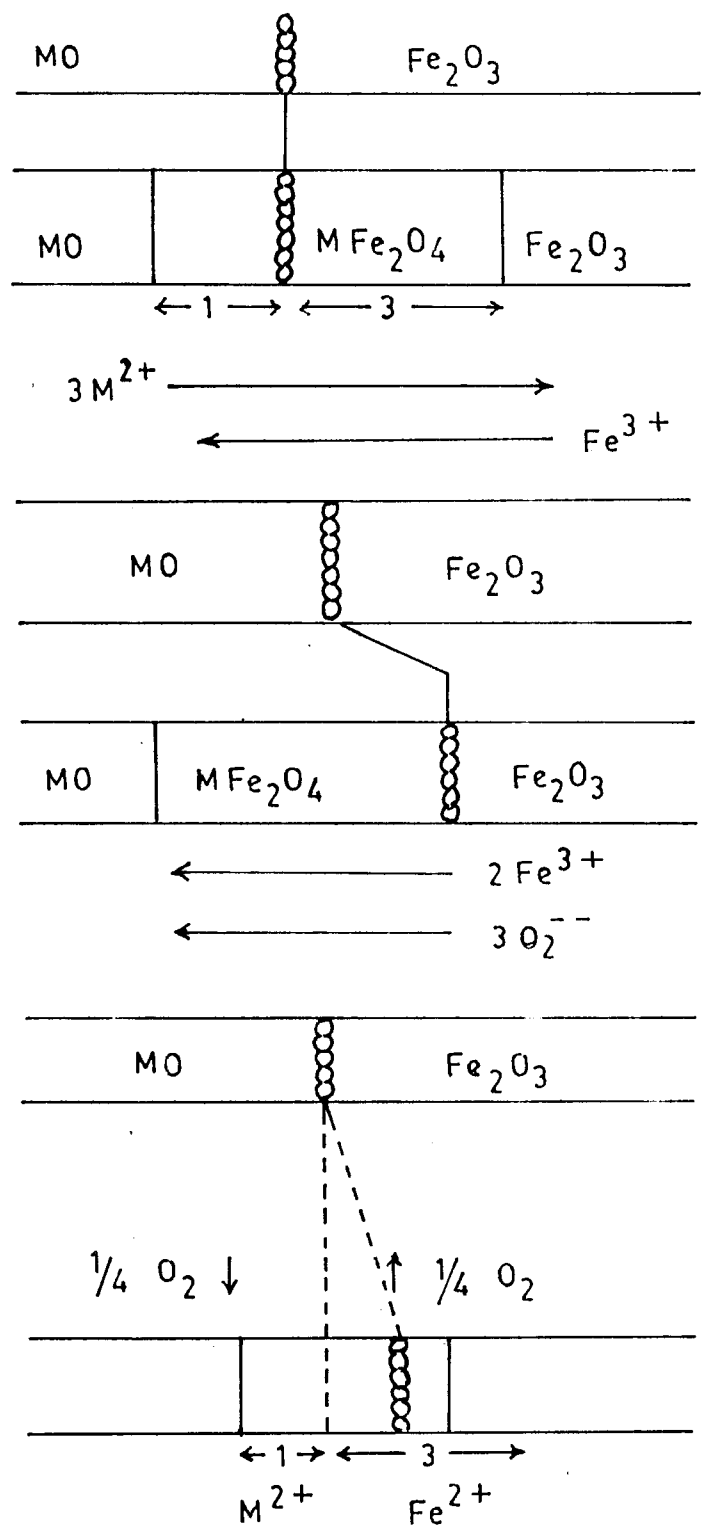
where MO = divalent metal oxide.

FIG. 2·⅄·3-Schematic representation of possible reaction mechanism involved in ferrite formation.

In the initial configuration there is only phase boundary between reactants. After the nucleation of the ferrite, this boundary is replaced by two different phase boundaries, one between MO and MFe_2O_4 and the other between Fe_2O_3 and MFe_2O_4. In this state, further progress of the reaction takes place by transport of reactants through the ferrite phase.

Three different mechanisms of transfer in which MFe_2O_4 may be formed are -

i.   Wagner[21] suggested the counter diffusion mechanism in which the cations migrate in opposite directions and the oxygen ions are essentially stationary. Under these conditions the positions of inert makers do not change.

e.g. The reaction between MgO and Fe_2O_3[24] to form $MgFe_2O_4$.

ii.   In the second model, the anions take part in the diffusion process. In this reaction diffusion of one cation, either Fe^{2+} or M^{2+}, is compensated by an associated flure of anions, instead of a counter current of another cation.

e.g. The reaction between ZnO and Fe_2O_3 to form $ZnFe_2O_4$[25]

iii.   In the third mechanism, iron diffuses through the ferrite layer in a reduced state Fe^{2+} as indicated by Paulus[26] and oxygen is transported through the gas phase. Oxygen

is evolved at MFe_2O_4/ Fe_2O_3 interface and taken up again at MO/MFe_2O_4 boundary.

e.g. The reaction between NiO and Fe_2O_3 to form $NiFe_2O_4$.

2.A.4   ACTUAL PREPARATION OF FERRITE SAMPLES

Ceramic method was used in the present work. The ferrites were prepared with the general formula -

$$Ni_x Cu_{0.2} Zn_{0.8-x} Fe_2O_4$$

where x = 0.2, 0.3, 0.4, 0.5, 0.6, 0.7 and 0.8

High purity oxides of nickel, zinc and copper were weighed in the required molar proportions and mixed mechanically in an agate mortor in acetone medium. The dry mixtures were then transferred into alumina crucible and were presintered at 800^0C for 10 hours. The presintered powders were subjected to hard milling process in acetone medium. The dried powders were sieved.

The dry powders were pressed in the form of pellets having 1 cm diameter and toroides of ID = 1 cm and OD = 1.5 cm using a hydraulic press with a pressure of 5 tons per square inch for five minutes.

The pellets and toroids were sintered at a temperature of 1150 ^0C for 24 hours in air medium. The pellets were removed from the furnace and polished.

PART - B : CHARACTERIZATION BY X-RAY DIFFRACTION

INTRODUCTION

X-ray diffraction plays an important role in ferrite research. The XRD is well established and used to -

i.   determine crystal structure

ii.   determine the lattice parameters, interplaner distance, octahedral and tetrahedral site radii and bond length etc.

iii. verify the completion of solid state reaction

iv.   study the crystal imperfections

Laue experimentally demonstrated the phenomenon of x-ray diffraction by crystals in 1912. The explanation of the observed diffraction pattern that results from x-rays was given by Bragg.[27] X-ray diffraction method developed by Bertaut[28], Warren and Aberbach[29] is applicable for the determination of a crystallite size distribution of materials.

2.B.1   X-RAY DIFFRACTION : PRINCIPLES

The diffraction maxima occur when Bragg law i.e.

$$2d \sin \theta = n\lambda \qquad \qquad \dots \quad (2.2)$$

where d = interplaner distance
$\quad \quad \theta$ = glancing angle
$\quad \quad$ n = order of diffraction
$\quad \quad \lambda$ = wave length of monochromatic x-rays
$\quad \quad \quad$ is satisfied
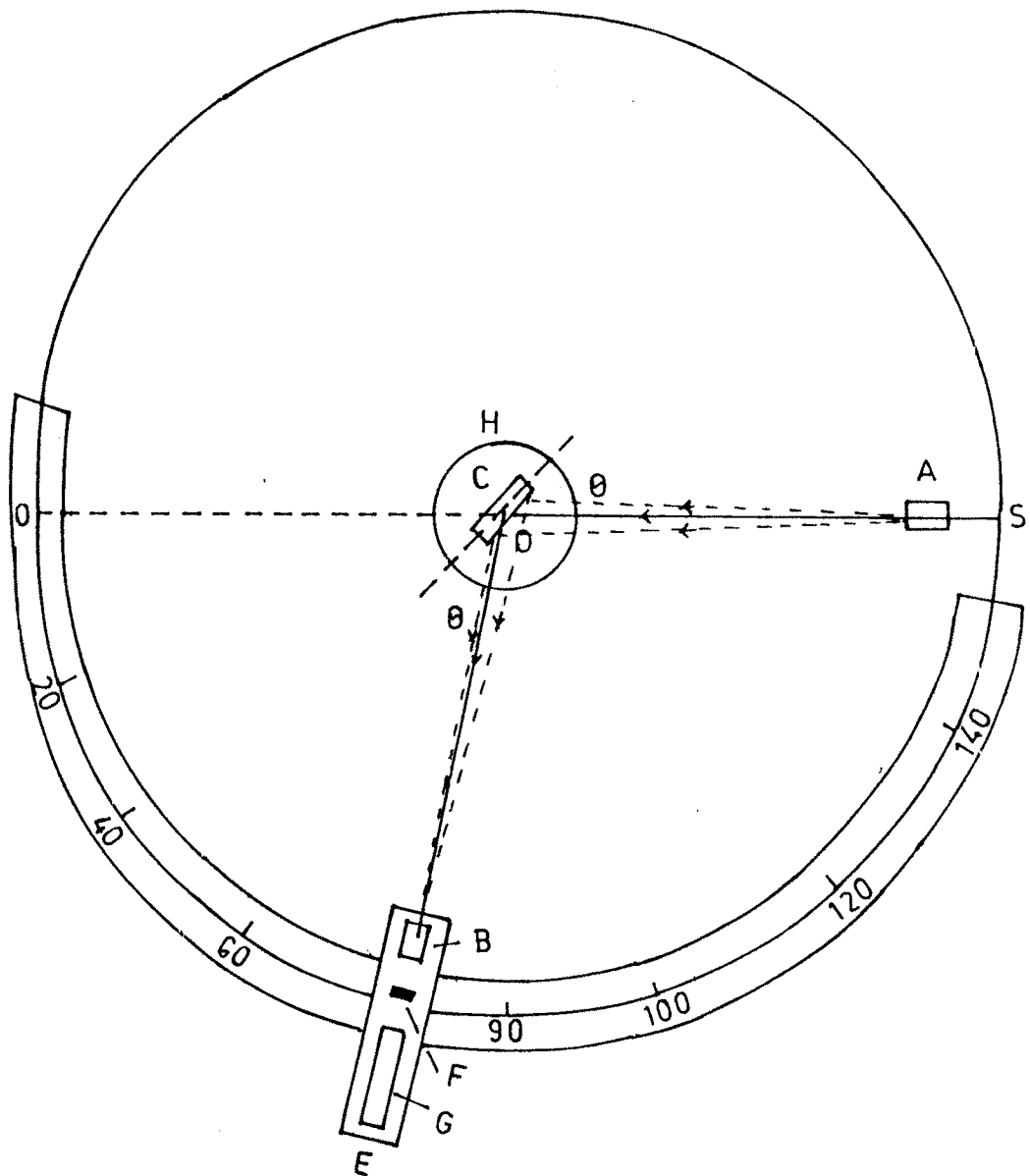
Diffractometer circle

FIG. 2·B·1 — X-ray diffractometer (Schematic) .

The schematic of x-ray diffractometer is shown in Fig. 2.B.1. The incident beam of x-rays is allowed to pass through the slit 'A' of the collimeter. As the crystallites are randomly oriented, a reflection at particular position is due to a set of atomic planes which satisfy Bragg condition. The diffracted beam gets converged and focused at slit 'F' which further enters the counter 'G'. With the help of special slit 'B' the diffracted beam is then collimated. The counter 'G' is connected to count rate meter and output of circuit is fed to a automatic recorder which registers count per second versus 2θ. The location of the centroid of the recorded peak gives 2θ, hkl for corresponding Bragg condition. The receiving slit and counter are supported on the carriage 'E' which can be rotated about the vertical axis through 'C' whose angular position 2θ can be read on circular scale 'K' as counter moves through 2θ degrees between 'E' and 'H'.

2.B.2   X-RAY DIFFRACTION METHODS

1.   Laue Method

This method is widely used to orient crystals for solid state experiments. In the Laue method, a single crystal is held stationary in a beam of white x-rays. Laue method enables us to investigate the structure of the crystal lattice and to determine the orientation of the crystal. The crystal selects and diffracts x-rays with discrete value of λ for which planes satisfy the Bragg's condition.

2. Rotating Crystal Method

In the rotating crystal method, a single crystal is rotated about a fixed vertical axis in a beam of monochromatic x-rays. The x-ray beam is diffracted from a given crystal plane satisfying the Bragg condition. The diffracted beams from the planes parallel to the vertical axis lie in the horizontal plane, whereas, those diffracted from the planes with other orientations reflect in layers above and below the horizontal plane.

3. Powder Method

Debye and Scherrer devised this method in 1916 in Germany. In this method, a finely powdered specimen is packed in a thin walled capillary tube and a monochromatic beam of x-ray is made to strike a specimen. The diffraction occurs from individual crystallites that are oriented with planes having same incident glancing angle 'θ'.

2.B.3 EXPERIMENTAL TECHNIQUES

The x-ray diffraction patterns of the samples in the present case were recorded using Cu K$\propto$ radiation of $\lambda = 1.5418$ A^0 on Philips diffractometer (model PW 1710).

The powder was spread uniformly on a mounted screen of sample holder so as to form a plane surface of the specimen. The chart speed was 1^0/min. The diffractograms were taken within the range of '2θ' angles between 20^0 and 80^0.

From the chart the values of 2θ are recorded and their corresponding 'd' values are calculated using the Bragg condition. In cubic system the interplaner distance 'd' is given by

$$d = \frac{a}{\sqrt{[h^2 + k^2 + l^2]}} \qquad \ldots \quad (2.3)$$

where a = lattice parameter

(hkl) = Miller indices

From equation (2.2)

$$d = \frac{n\lambda}{2 \sin \theta} \qquad \ldots \quad (2.4)$$

By comparing equation (2.3) and (2.4) we get

$$\frac{a}{\sqrt{h^2 + k^2 + l^2}} = \frac{n\lambda}{2 \sin \theta} \qquad \ldots \quad (2.5)$$

$$\therefore \quad a = \frac{\lambda}{2 \sin \theta} (h^2 + k^2 + l^2)^{1/2} \qquad \ldots \quad (2.6)$$

The prominent line in the diffraction pattern of spinels corresponds to (311) plane. The value of θ corresponding to (311) plane was noted from the chart. Substituting the value of $\sin \theta$, (hkl) and 'λ' in equation (2.6), lattice parameter was calculated. By knowing the values of 'a' and (hkl), 'd' values for other planes were calculated by usual procedure.

The following relations were used to calculate the bond length of tetrahedral (R_A) and octahedral (R_B) sites.

$$R_A = a\sqrt{3}\ (\delta + {}^1/_8) \qquad \dots \quad (2.7)$$

$$R_B = a\sqrt{3\delta^2 + {}^1/_{16} - \delta/2} \qquad \dots \quad (2.8)$$

where $\delta = u - 0.375$

$$u = \frac{u_1 + u_2}{2}$$

$u_1 = 0.381\ A^0$ for $NiFe_2O_4$, $u_2 = 0.385\ A^0$ for $ZnFe_2O_4$

The site radii were calculated using the relations

$$r_A = a.\sqrt{3}\ .\ (u - {}^1/_4) - ro \qquad \dots \quad (2.9)$$

$$r_B = a.\ ({}^5/_8 - u) - ro \qquad \dots \quad (2.10)$$

where ro = radius of oxygen ion = $1.35\ A^0$

2.B.4   RESULTS AND DISCUSSION

The x-ray diffraction patterns for the present samples with the general formula $Ni_x\ Cu_{0.2}\ Zn_{0.8-x}Fe_2O_4$ (where x = 0.2, 0.3, 0.4, 0.5, 0.6, 0.7, 0.8) are shown in Figs. 2.B.2 to 2.B.8. It can be seen that all samples exhibit cubic spinel structure. The diffraction maxima have been indexed in the light of spinel structure. The reflections observed are (220), (311), (400), (511), (440), (533) etc. These correspond to the allowed values of reflections for cubic spinel structure. From the diffraction pattern it is observed that the plane

that the lattice parameter decreases with increasing nickel content (decrease in Zn content) which is attributed to the smaller ionic radius of Ni^{2+} than that of Zn^{2+}. The relationship between the ionic radius and lattice constant is well established.[31] It can also be observed that the Vegard's law is obeyed for the present system. Pascand et.al.[32] have found that the distance between the magnetic ions on A site increases with the introduction of larger ions in the Nix $Zn_{1-x}Fe_2O_4$ system.

A similar linear variation of lattice parameter with Zn content has been reported[33] for the MZn ferrites (where M = Ni, Co, Cu, Mg). The reported values of lattice parameters for $Ni_{1-x}Zn_xFe_2O_4$ and for $Ni_{0.9-x}Cu_{0-1}Zn_xFe_2O_4$ are $8.33A^0$ to $8.45A^0$ and $8.34A^0$ to $8.43A^{034}$ respectively. The present values of lattice parameter lie within this range.

Kakatkar et.al.[35] have done XRD studies of Ni-Zn ferrites sintered at different temperatures and observed that the lattice parameter increases linearly with Zn^{2+} content, which they have attributed to large ionic radius of Zn^{2+}.

From Fig. 2.B.10, it is observed that on addition of Ni^{2+} the bond lengths R_A and R_B decrease. The linear decrease of R_A and R_B with Ni is attributed to the decrease of lattice parameter. Lavine[36] has co-related the decrease in bond length to an increase in covalent
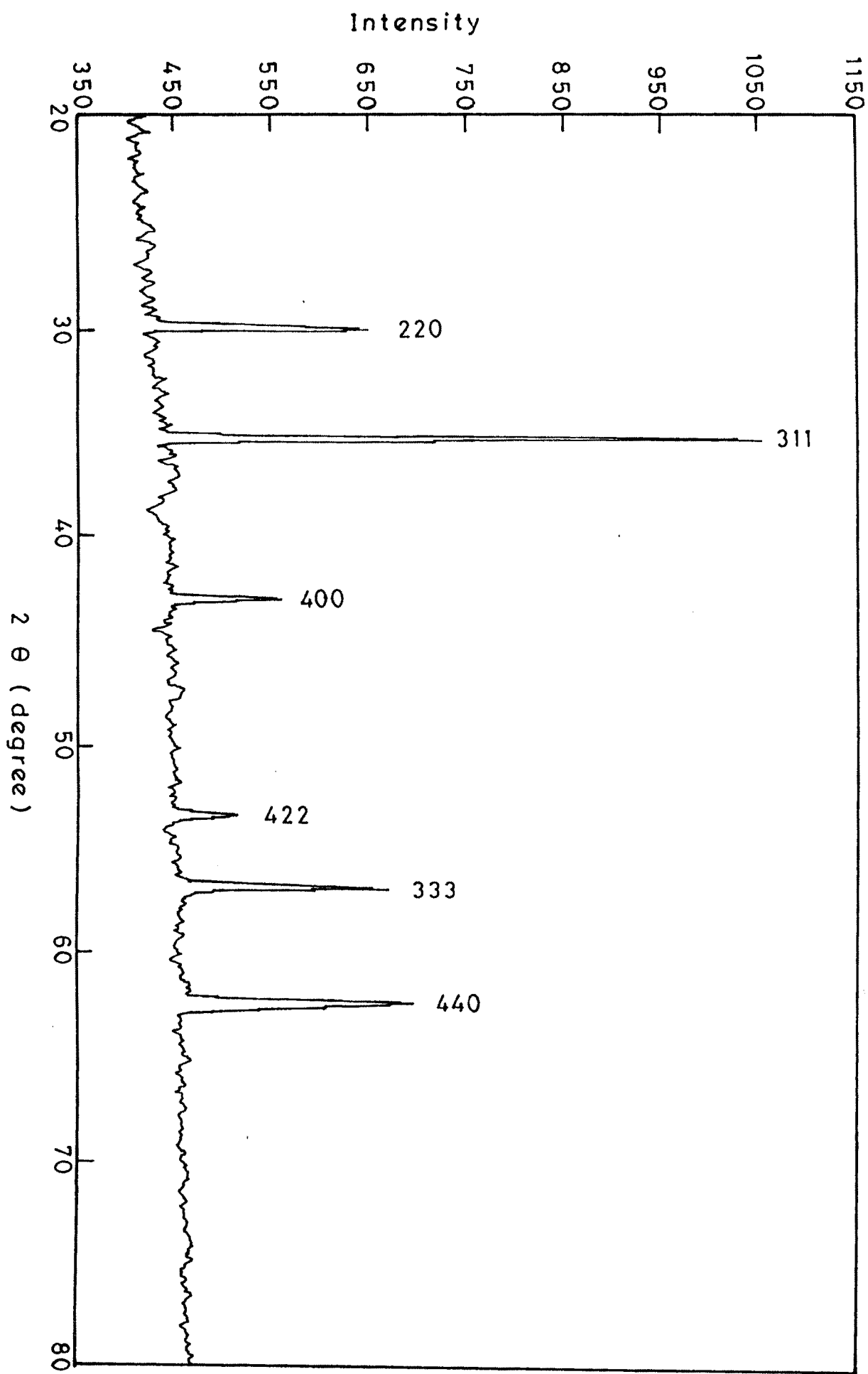
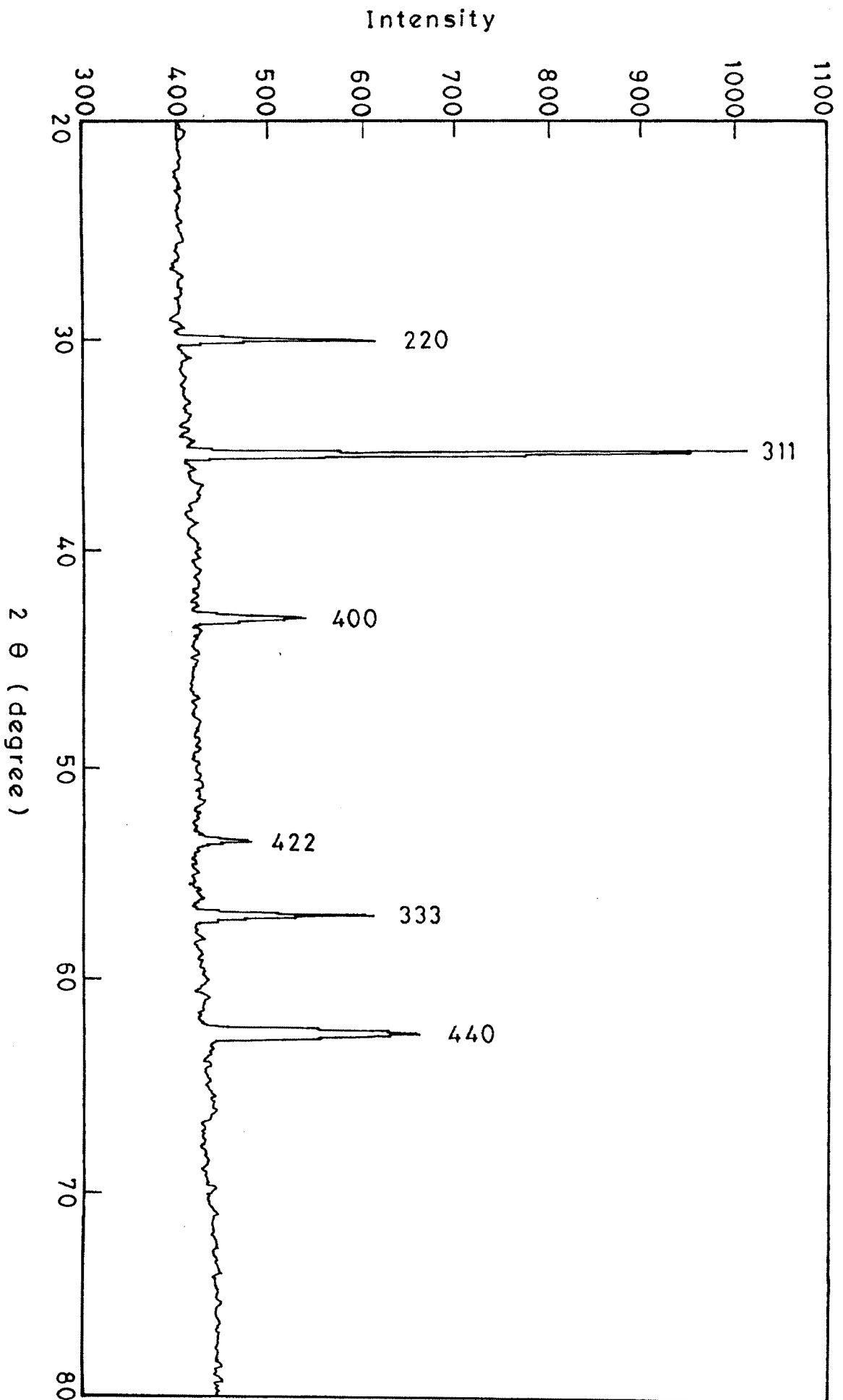FIG.2-B-2 - X-RAY DIFFRACTION FOR $Ni_{0.2}Cu_{0.2}Zn_{0.6}Fe_2O_4$ FERRITE.

FIG. 2-B-3-X-RAY DIFFRACTION FOR Ni$_{0.3}$Cu$_{0.2}$Zn$_{0.5}$Fe$_2$O$_4$ FERRITE.

FIG.2-B-4—X-RAY DIFFRACTION FOR Ni$_{0.4}$Cu$_{0.2}$Zn$_{0.4}$Fe$_2$O$_4$ FERRITE.
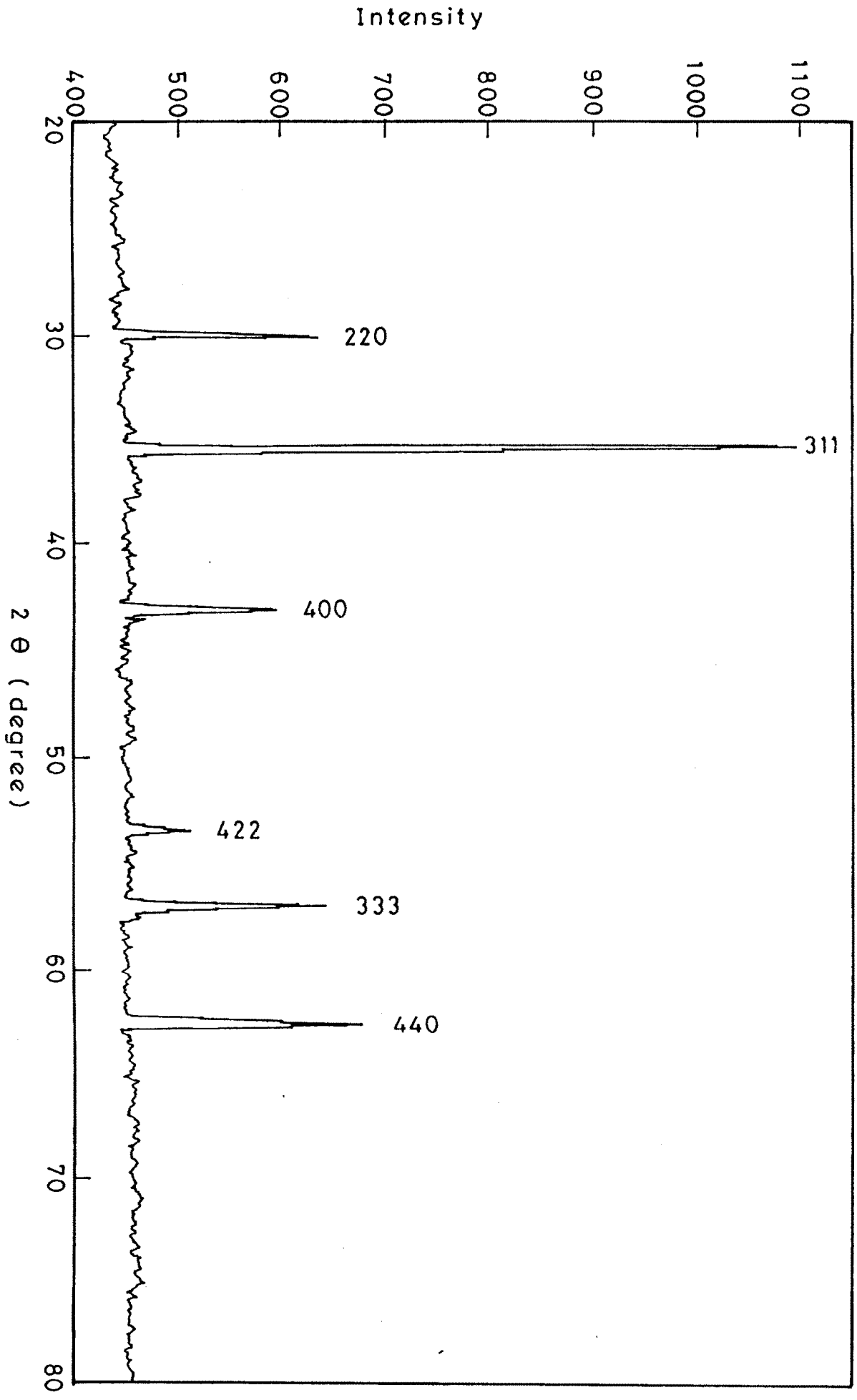
FIG. 2·B·5 - X - RAY DIFFRACTION FOR $Ni_{0.5} Cu_{0.2} Zn_{0.3} Fe_2O_4$ FERRITE.
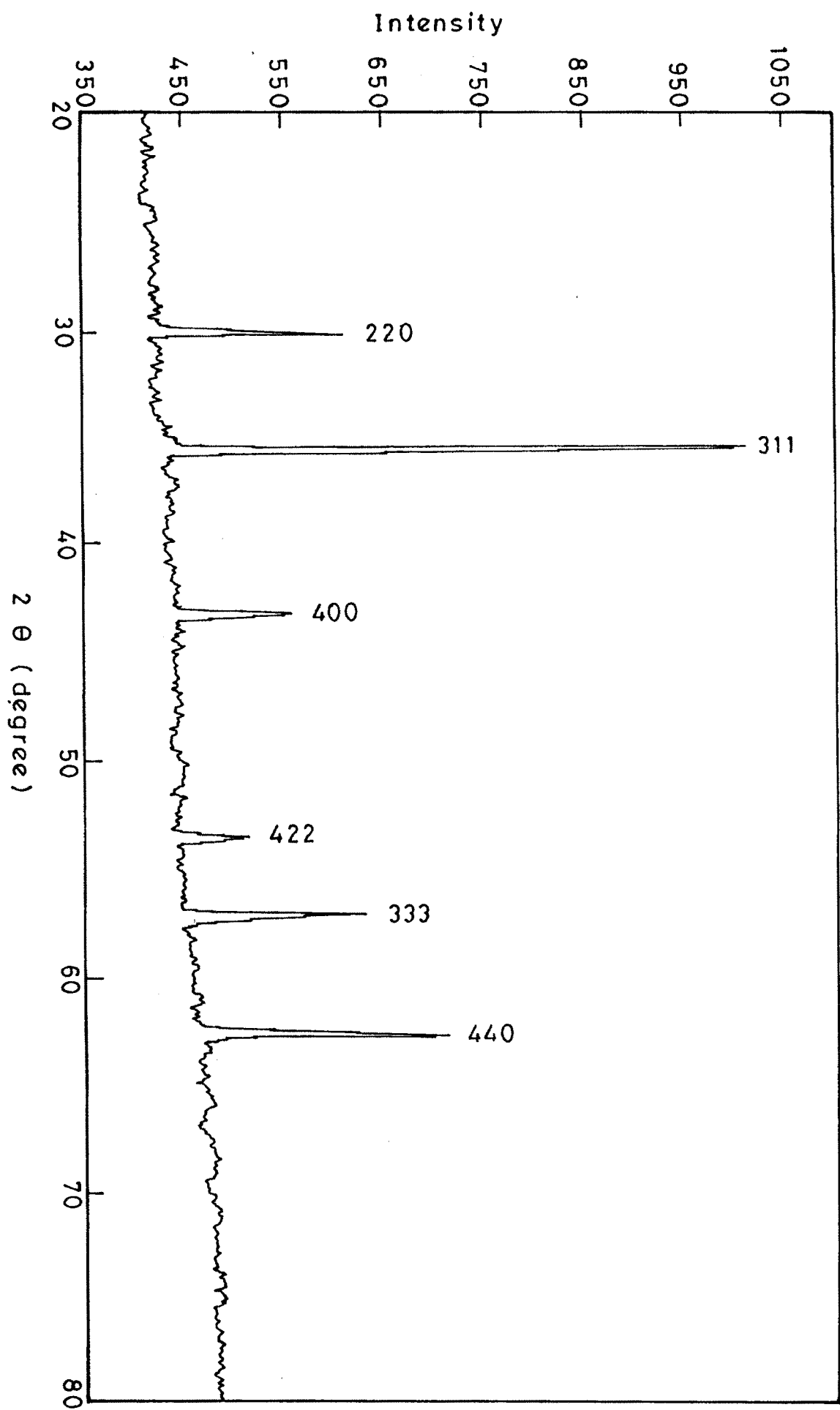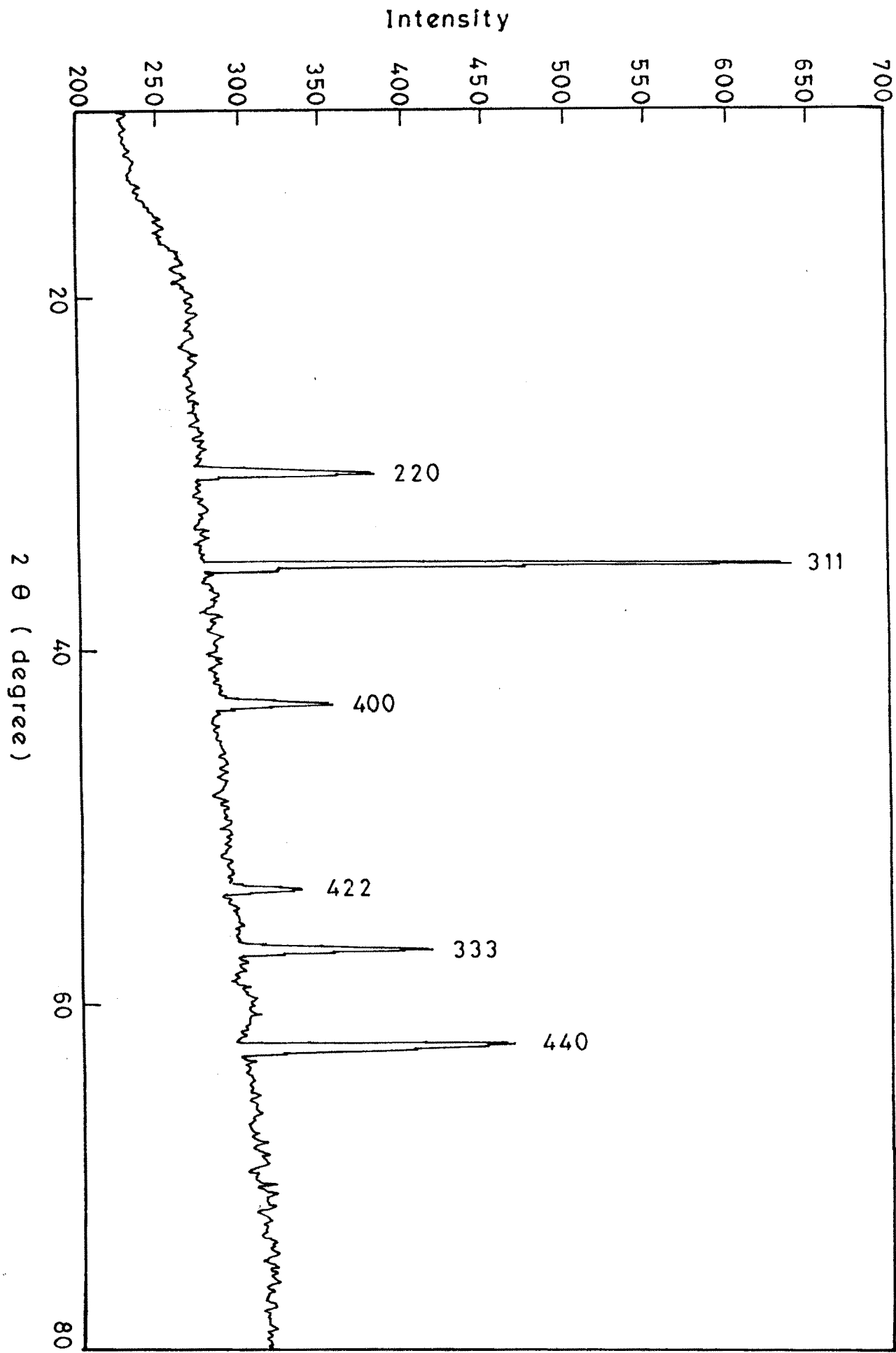
FIG.2.B.6.X-RAY DIFFRACTION FOR Ni$_{0.6}$Cu$_{0.2}$Zn$_{0.2}$Fe$_2$O$_4$ FERRITE.

FIG. 2·B·7 - X RAY DIFFRACTION FOR Ni$_{0.3}$Cu$_{0.7}$Zn$_{0.1}$Fe$_2$O$_4$ SAMPLE
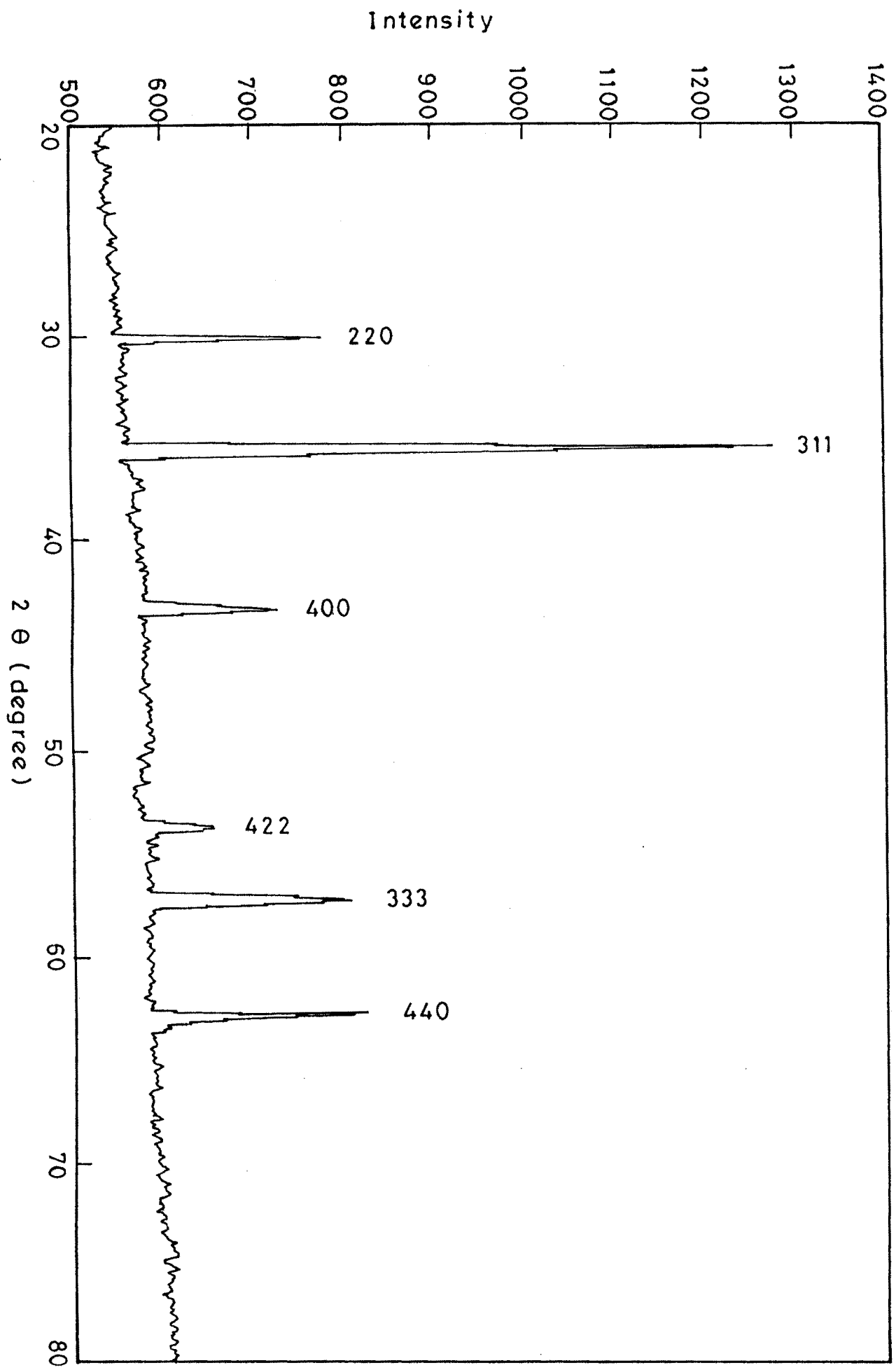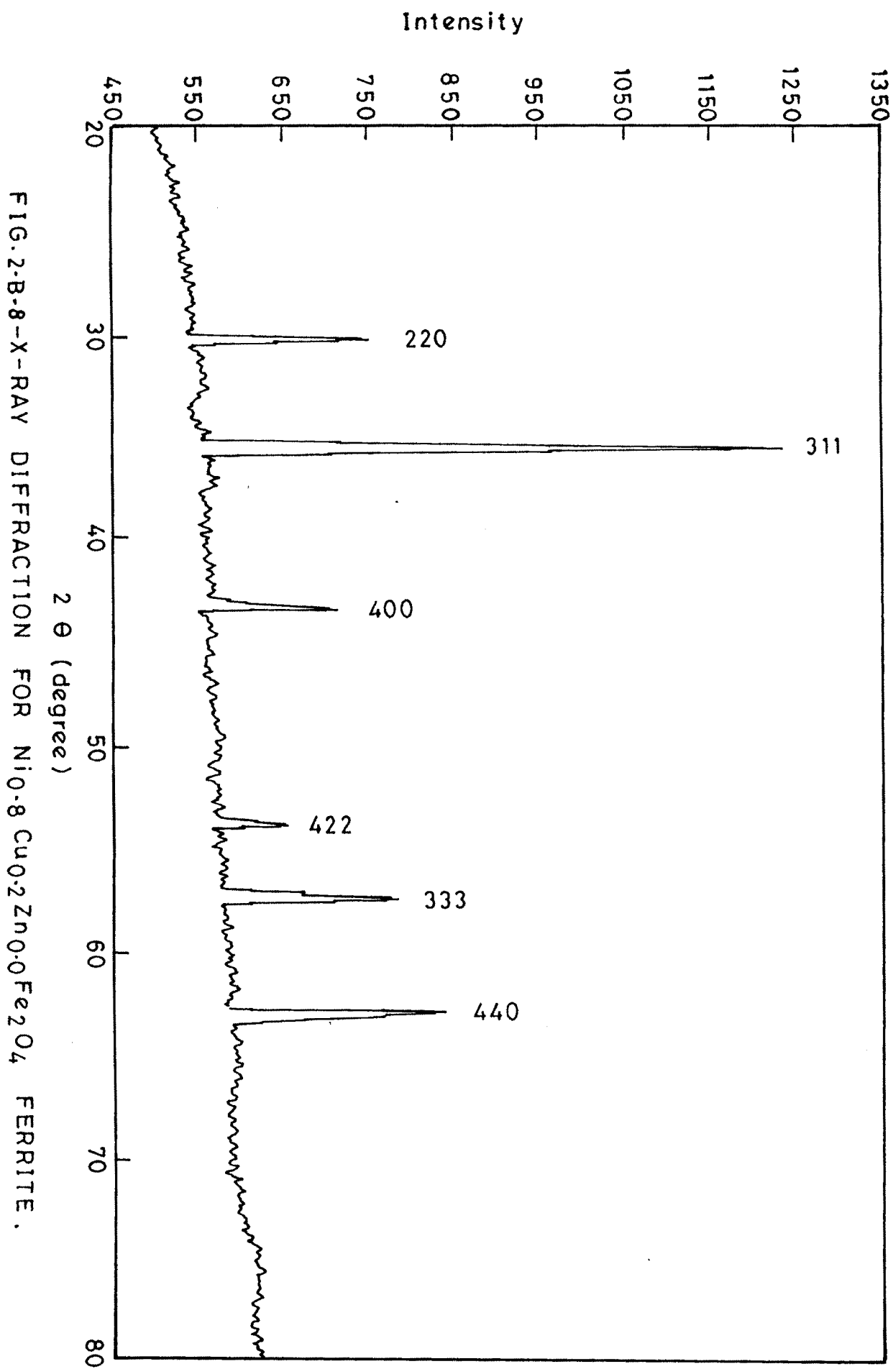
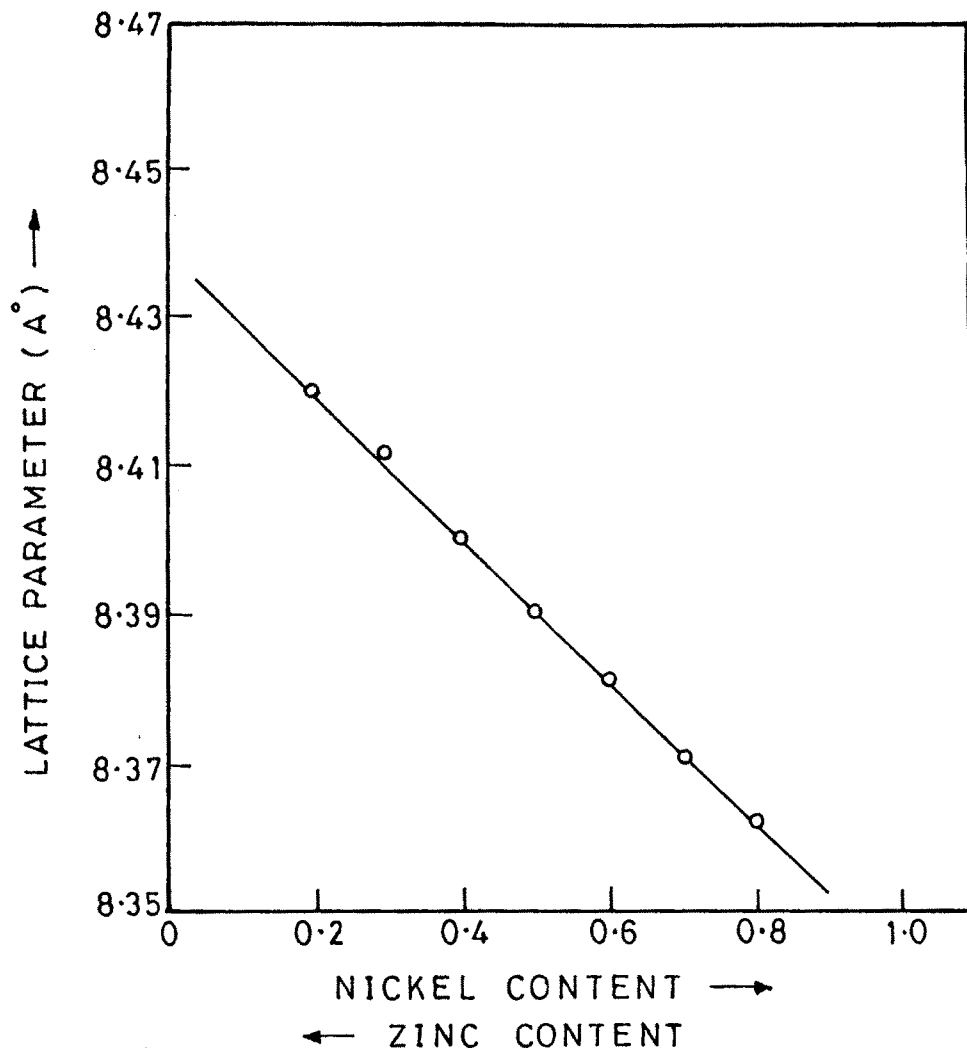FIG.2-B-8-X-RAY DIFFRACTION FOR Ni0·8 Cu0·2Zn0·0Fe2O4 FERRITE.

FIG. 2·B·9 – VARIATION OF LATTICE PARAMETER WITH NICKEL CONTENT FOR $Ni_x Cu_{0.2} Zn_{0.8-x} Fe_2 O_4$ FERRITES.
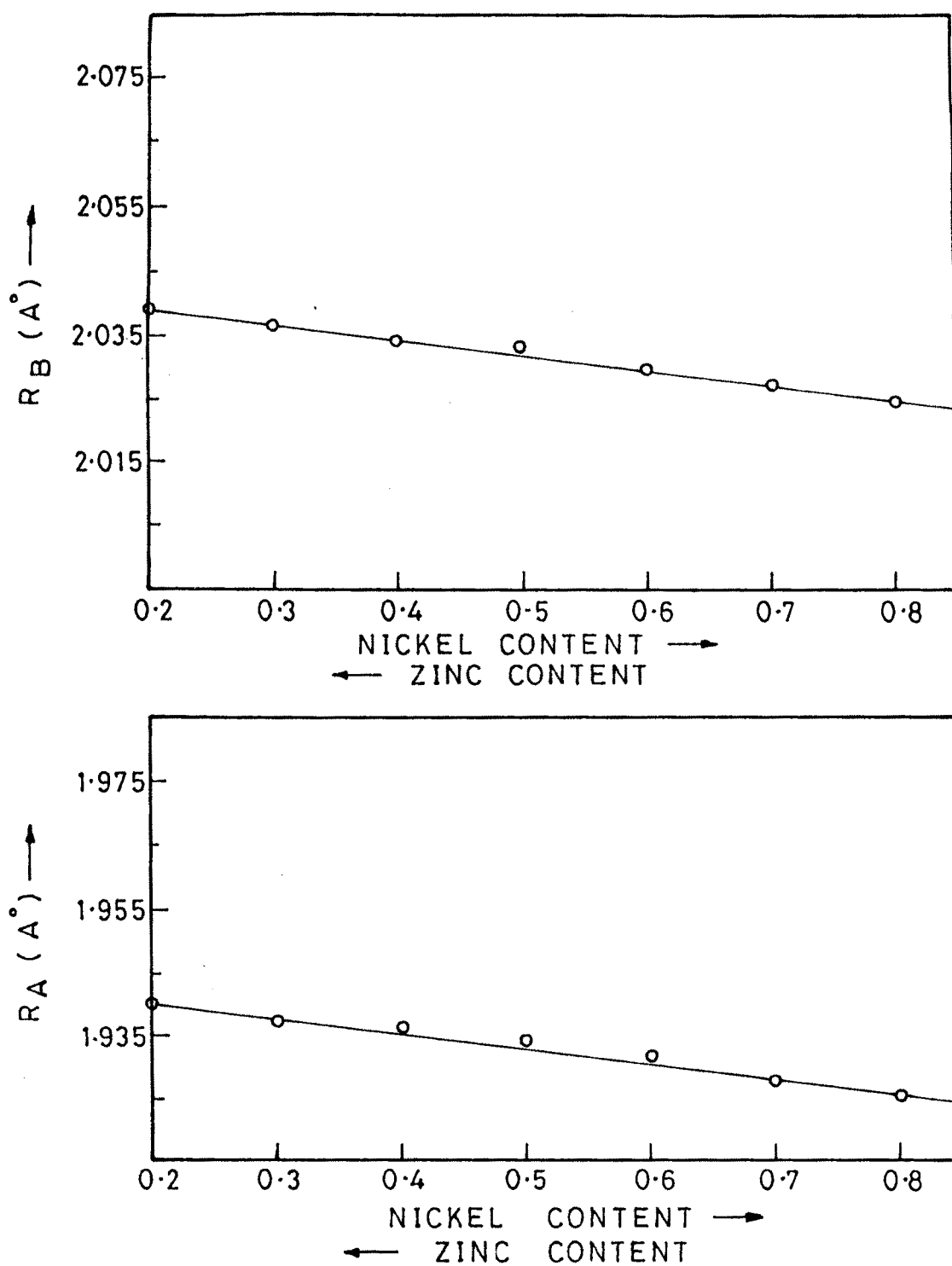
FIG. 2·B·10 − VARIATION OF BONDLENGTH WITH NICKEL CONTENT FOR $Ni_x Cu_{0.2} Zn_{0.8-x} Fe_2 O_4$ FERRITES.
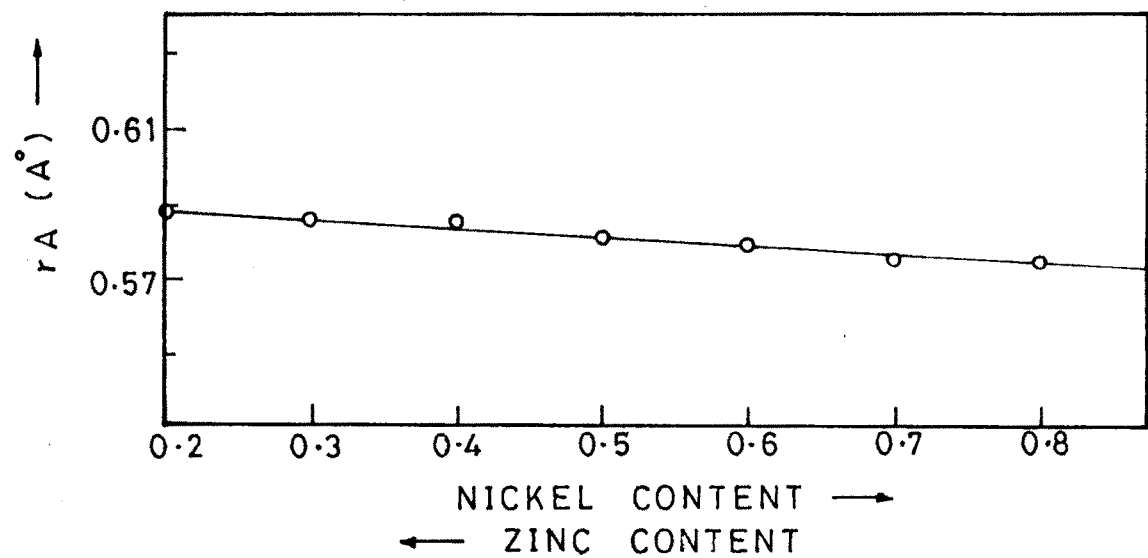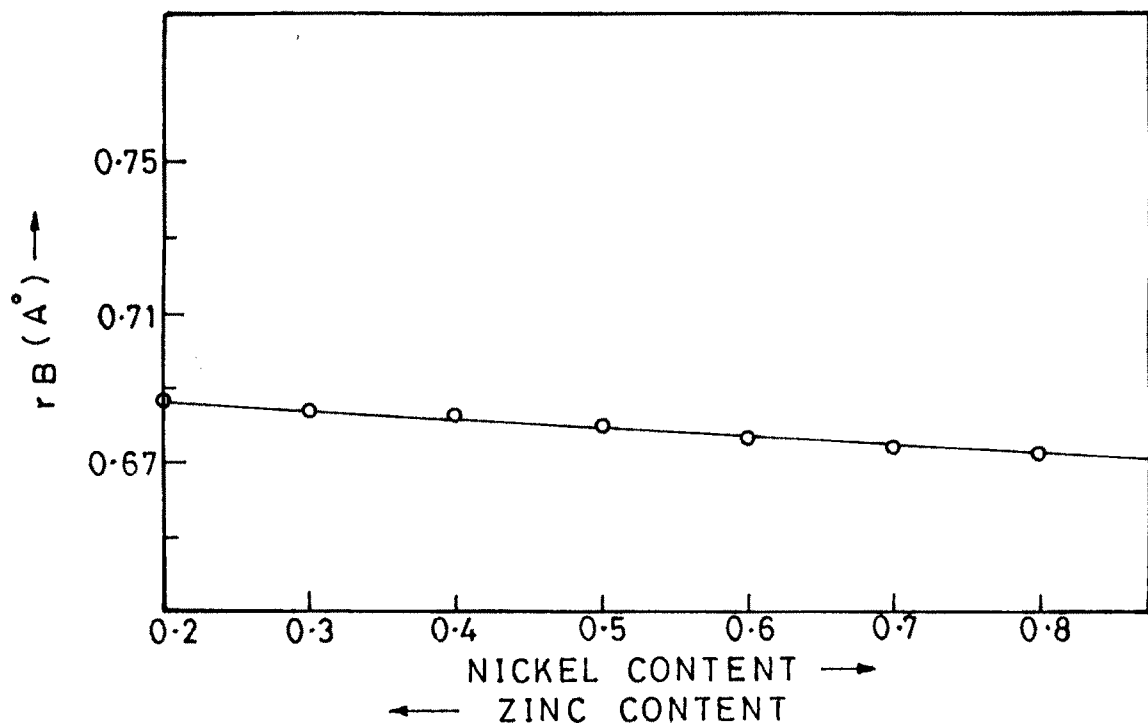
FIG. 2·B·11 — VARIATION OF SITE RADII WITH NICKEL CONTENT FOR $Ni_x Cu_{0.2} Zn_{0.8-x} Fe_2 O_4$ FERRITES.

Table 2.B.1 X-ray diffraction data of $Ni_{0.2} Cu_{0.2} Zn_{0.6} Fe_2O_4$ ferrite
$a = 8.420$ A^0

(hkl)	d_{cal}, A^0	d_{obs}, A^0
220	2.977	2.980
311	2.539	2.540
400	2.105	2.106
422	1.719	1.719
333	1.620	1.617
440	1.488	1.486

Table 2.B.2 X-ray diffraction data of $Ni_{0.3} Cu_{0.2} Zn_{0.5} Fe_2O_4$ ferrite

$a = 8.414$ A^c

(hkl)	d_{cal}, A^0	d_{obs}, A^0
220	2.973	2.979
311	2.536	2.534
400	2.103	2.100
422	1.717	1.715
333	1.619	1.619
440	1.487	1.487

Table 2.B.3 X-ray diffraction data of $Ni_{0.4}Cu_{0.2}Zn_{0.4}Fe_2O_4$ ferrite

$a = 8.401 \ A^0$

(hkl)	$d_{cal}, \ A^0$	$d_{obs}, \ A^0$
220	2.969	2.969
311	2.533	2.536
400	2.100	2.102
422	1.715	1.714
333	1.617	1.618
440	1.485	1.486

Table 2.B.4 X-ray diffraction data of $Ni_{0.5}Cu_{0.2}Zn_{0.3}Fe_2O_4$ ferrite

$a = 8.390 \ A^0$

(hkl)	$d_{cal}, \ A^0$	$d_{obs}, \ A^0$
220	2.966	2.965
311	2.530	2.533
400	2.098	2.098
422	1.713	1.714
333	1.615	1.616
440	1.483	1.484

Table 2.B.5 X-ray diffraction data of $Ni_{0.6} Cu_{0.2} Zn_{0.2} Fe_2O_4$ ferrite
$a = 8.383$ A^0

(hkl)	d_{cal}, A^0	d_{obs}, A^0
220	2.977	2.980
311	2.539	2.540
400	2.105	2.106
422	1.719	1.719
333	1.620	1.617
440	1.488	1.486

Table 2.B.6 X-ray diffraction data of $Ni_{0.7} Cu_{0.2} Zn_{0.1} Fe_2O_4$ ferrite
$a = 8.372$ A^0

(hkl)	d_{cal}, A^0	d_{obs}, A^0
220	2.959	2.956
311	2.524	2.524
400	2.093	2.092
422	1.709	1.708
333	1.611	1.611
440	1.479	1.479

Table 2.B.7 X-ray diffraction data of $Ni_{0.8} Cu_{0.2} Zn_{0.0} Fe_2O_4$ ferrite
   $a = 8.364$ A^0

(hkl)	d_{cal}, A^0	d_{obs}, A^0
220	2.956	2.958
311	2.521	2.518
400	2.090	2.090
422	1.707	1.706
333	1.609	1.608
440	1.478	1.477

Table 2.B.8 Data on lattice parameters, bond length and site radii for $Ni_x Cu_{0.2} Zn_{0.8-x} Fe_2O_4$ ferrites

χ	$a\ A^0$	$R_A\ A^0$	$R_B\ A^0$	$r_A\ A^0$	$r_B\ A^0$
0.2	8.420	1.939	2.039	0.589	0.687
0.3	8.414	1.937	2.036	0.587	0.684
0.4	0.401	1.936	2.035	0.586	0.683
0.5	8.390	1.934	2.033	0.582	0.681
0.6	8.383	1.930	2029	0.579	0.677
0.7	8.372	1.927	2.027	0.577	0.675
0.8	8.364	1.925	2.024	0.575	0.672

Table 2.B.9 Ionic radii of cations

Cation	Zn^2	Ni^2	Fe^3	Cu^2
Ionic radius A^0	0.83	0.74	0.67	0.72

Table 2.B.10 Data on molecular weight (M), actual density (da), X-ray density (dx) and porosity (Po) for $Ni_xCu_{0.2}Zn_{0.8-x}$ Fe_2O_4 Ferrites

x	M gm mol	da gm/ cc	dx gm/ cc	Po,%
0.2	239.26	4.58	5.30	14
0.3	238.69	4.59	5.33	14
0.4	238.02	4.53	5.33	15
0.5	237.36	4.73	5.34	11
0.6	236.68	4.77	5.34	10
0.7	236.02	4.45	5.35	16
0.8	235.35	4.78	5.35	11

(311) is more intense in all the samples. There are no extra lines present in the XRD patterns indicating the formation of a single phase spinel structure.

The interplaner distance 'd' was calculated for each line with respect to the line of maximum intensity viz. (311). The observed and calculated 'd' values and Miller indices are presented in Tables 2.B.1 to 2.B.7. It is observed that the observed and calculated 'd' values are in good agreement with each other.

By using the relation 2.5 the lattice parameter was calculated for each sample. Using these values of lattice parameter in relation (2.7) and (2.8), the values of bond lengths (R_A and R_B) were calculated. By using relation (2.9) and (2.10), the site radii (r_A and r_B) were calculated. The data on composition, lattice parameter, bond length and site radii is presented in Table 2.B.8. Table 2.B.9 gives the data on ionic radii of the cations involved. Table 2.B.10 lists molecular weight, actual density (da), x-ray density (dx) and porosity values of the samples.

The samples of $Ni_x Cu_{0.2} Zn_{0.8-x} Fe_2O_4$ ferrite system exhibit cubic structure in agreement with the results reported by Srivastava et.al.[30]

Fig.2.B.9 shows the compositional variation of lattice parameter with content of nickel for the present ferrites. It is seen

character of the ferrite. In the present system, an increase in Ni content, results in decrease in the covalent character of the ferrite. Bond lengths exhibit a sensitive dependence on covalancy and composition[37] Patil et.al.[37] have reported increase in R_A and R_B with x in $Mn_x Zn_{o.3} Ni_{0.7-x} Fe_{2-2x}O_4$. This may be due to changes in the valancies of Mn and Ni.

From Fig. 2.B.11 it is seen that site radii r_A and r_B also decrease with increasing Ni content. This is attributed to larger ionic radius of Ni^{2+} than that of Fe^{3+}.

Table2B.10 gives the values of x-ray density (dx) and actual density (da). The observed density is lower than the x-ray density and close to reported values for Mn- Zn ferrites.[38] In the present work the porosity lies between 10 to 16%.

REFERENCES

1. Goldman, A.
    "MODERN FERRITE TECHNOLOGY",
    Van Nostrand Reinhold, New York. Fresh D.L., "Methods of preparation and crystal Chemistry of Ferrites", Proc. IRE, 44 (1956) 1303-41

2. Johnson Jr. D.W. and Ghate B.B.
    "SCIENTIFIC APPROACH TO PROCESSING OF FERRITES" pp. 27-38 in Advances in Ceramics, Vol. 15, Fourth International Conference on Ferrites, Part-I edited by F.F.Y. Wang, American Ceramic Society, Columbus, OH (1986)

3. Ross E.
    "MODERN TECHNOLOGY FOR MODERN FERRITE",
    pp. 129-36 in proceeding of Fifth International Conference on Ferrites, Advances in Ferrites. Edited by Srivastava C.M. and Patni M.J., Oxford and JBM Publishing Co.

4. Hilpert S.
    Ber. Deut. Chem. Ges 42 (1909) 2248

5. Hedvall J.A.
    Ber. Deut. Chem. Ges 45 (1912) 2095

6. Tammann G.
    Z. Anorg. Allgen. Chem. 78(1921) 111

7. Jandar,
    Z. Anorg. Allgen. Chem. (1927) 1631

8. Wagner C.
    "Diffusion and High temperature oxidation of metals, atomic movements", Z. Phys. Chem. (B) 34 (1936) 306

9. Takei T., Sugimoto M. and Okamoto S.
    "FERROMAGNETIC OXIDE MATER", Japan Pat. No. 202, 893 (1953)

10. Takei T. and Sugimoto M.
"SINTERING OF BA-BI FERRITES". Sci. Pap. Inst. Phys. Chem. Res. (Jpn) 54, 212-18 (1960)

11. Van Uitert L.G.
"High-Resistivity Nickel Ferrites- The Effect of Minor Addition of Manganese or Cobalt", J. Chem. Phys. 24 (1956) 306

12. Economus G.
J. Amer. Ceram. Soc. 38 (1955) 241

13. Wolf W.P. and Rodrigue G.P.
J. Appl. Phys. 29 (1958) 105

14. Sato T.
IEEE Trans. Magn. 6 (1970) 765

15. Sato T., Kuroda C. and Sato M.
"Ferrites" Proc. I.C.F., Kyoto, Tokyo (1970) 72

16. Busev A.I., Kohraya N.V., Korastelev P.P. and Mikhialev G.K.
Inorg. Mater (USA) 16, 10 (1980) 1842

17. Rikukawa H. and Sasaki I.,
"COMPUTER-AIDED ENGINEERING FOR FERRITE PRODUCTS", J. Phys. IV (Paris) Suppl. III) (1997) 133

18. Swallow D. and Jorden A. K.
Proc. Brit. Ceramic Soc. 2 (1964) 1

19. Coble A.L. and Koop C.
Sci. Ceramic 2 (1965) 231

20. Wagner C.
"Influsion and High temperature oxidation of Metals : Atom movements". A.S.M. Monographs (Cleavland) (1951), 153. Z. Phys. Chem. (B) 34 (1936) 309

21. Schmalzried H.
Z. Phys. Chem. (NF) 35 (1962) 111

22. Reijnen P.
Sci. Ceram. 42 (1956) 143

23. Carter R.E.
J. Amer. Chem. Soc. 44 (1961) 116

24. Economos G.
"KINETICS OF HIGH TEMPERATURE PROCESSING",
Kingery W.D. Ed. M.I.T. press, Cambridge (1959) 243

26. Paulus M.
Proc. ICF, Kyoto, Japan (1970)

27. Bragg W.L.
Nature (London) 95 (1915) 561

28. Bertaut M.F.
Compt. Rend. 228 (1949) 492

29. Warren B.E. and Aberbach B.L.
J. Appl. Phys. 21 (1950) 595

30. Srivastava C.M., Patani M.J. and Srinivasan T.T.
J. Appl. Phys. 53 (1982) 2107

31. Vermass F.H.S. and Schmidt E.R.
Beit. Mineral Petrogra, 6 (1959) 219

32. Pascand H., Globus A. and Caban V.
J. Phys (Paris) Colloq., 38 C-1 (1977) 68

33. Ramana Moorthy S., Revati B. and Rao, T.S.
J. Less. Comm. Metals, 57 (1978) 29

34. Joshi G.K., Khot A.Y. and Sawant S.R.
Indian J. Phys. 62A (1988) 348

35. Kakatkar S.V., Kakatkar S.S., Patil R.S., Sankapal A.M., Suryawanshi S.S., Bhosale D.N. and Sawant S.R.
Phys. Status Solidi (b), 198 (1996) 853

36. Levine B.F.
Phys. Rev. B 87 (1973) 2591

37. Bhise B.V., Dongare M.B., Patil S.A.and Sawant S.R.
J. Mater. Sci. Lett. 10 (1991) 922

38. Chaudhari N.D.
Ph.D. Thesis, Shivaji University, Kolhapur (1998)